PanoNormal: Monocular Indoor 360° Surface Normal Estimation

Kun Huang[1], Fanglue Zhang[1], and Neil Dodgson[1]

School of Engineering and Computer Science, Victoria University of Wellington
{Kun.Huang,Fanglue.Zhang,Neil.Dodgson}@vuw.ac.nz

Abstract. The presence of spherical distortion on the Equirectangular image is an acknowledged challenge in dense regression computer vision tasks, such as surface normal estimation. Recent advances in convolutional neural networks (CNNs) strive to mitigate spherical distortion but often fall short in capturing holistic structures effectively, primarily due to their fixed receptive field. On the other hand, vision transformers (ViTs) excel in establishing long-range dependencies through a global self-attention mechanism, yet they encounter limitations in preserving local details. We introduce *PanoNormal*, a monocular surface normal estimation architecture designed for 360° images, which combines the strengths of CNNs and ViTs. Specifically, we employ a multi-level global self-attention scheme with the consideration of the spherical feature distribution, enhancing the comprehensive understanding of the scene. Our experimental results demonstrate that our approach achieves state-of-the-art performance across multiple popular 360° monocular datasets. The code and models will be released.

1 Introduction

Estimating surface normal is a crucial task in computer vision as it provides essential geometric information about the structure and orientation of surfaces within a scene. By offering valuable insights into the underlying 3D geometry of objects, accurate surface normal estimation contributes significantly to advancing the capabilities of a wide range of applications, including object recognition, autonomous driving, and robotics. Despite significant progress in normal estimation for conventional perspective images [4, 16], the task of 360° normal estimation remains less explored. When directly applying the methods proposed for perspective images to 360° images, the results are unsatisfactory. This is because the spatial warping inherent in 360° images is not taken into account in these techniques and so we instead, in this paper, develop specialized techniques tailored to their spherical representation.

To solve the distortions in panoramas in other similar tasks such as 360° depth estimation, some works have proposed projection-fusion architectures such as UniFuse [13] to leverage complementary information from the equirectangular projection (ERP) image and cubemap projection (CMP) patches to refine prediction outcomes in the spherical domain. However, this strategy needs to bridge
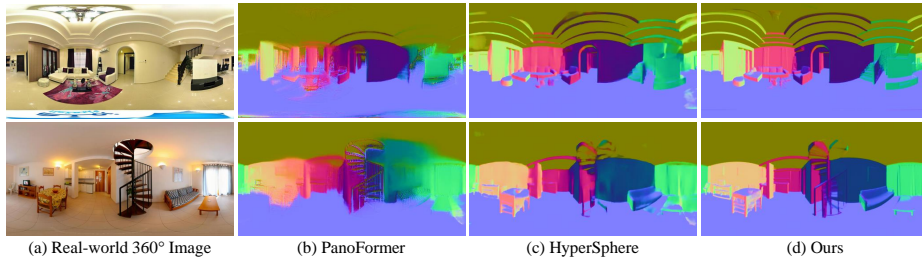
(a) Real-world 360° Image   (b) PanoFormer   (c) HyperSphere   (d) Ours

Fig. 1: Normal estimation results on real-world instances and previously unseen data from SUN360 [23]. Our approach, when compared to (b) PanoFormer [18] and (c) HyperSphere [14], stands out for its ability to provide precise surface normal details, even in challenging scenarios.

the domain gap between different projections, and the additional cross-projection fusion module introduces extra computational overhead. Distortion-aware deep learning frameworks are also proposed to mitigate such issues [8,16], embedding spherical geometry explicitly or implicitly into CNNs, or devising specialized loss functions tailored for panoramic images. More recently, researchers have adopted self-attention mechanisms to recapture a holistic understanding of the entire scene within the 360° domain [15,18]. While CNNs demonstrate prowess in localized feature extraction, they exhibit limitations in preserving the holistic structure of the 360° scene. Conversely, transformers guarantee the modelling of long-range dependencies but show shortcomings in capturing fine-grained details. Furthermore, conventional transformer-based methods cannot reveal the inherent spherical properties of the input signal. These limitations of CNNs and transformers led us to investigate hybrid architectures that seamlessly integrate the strengths of both for 360° images, fostering a refined and comprehensive representation of the scene across diverse scales for 360° surface normal estimation.

In this paper, we present *PanoNormal*, a framework for monocular surface normal estimation in 360° indoor environments. *PanoNormal* strategically integrates the strengths of CNNs for extracting low-level features and enhancing locality, along with the advantages of transformers in capturing and associating long-range dependencies. We introduce a deep learning module aimed at extracting low-level features from raw 360° images, departing from the conventional approach of direct tokenization inputs. To enhance the capabilities of self-attention in exploring the structure of the surface normal map, we propose a multi-scale transformer decoder, enriching the final representation by integrating information across diverse scales. In Fig. 1, previous state-of-the-art methods deliver sub-optimal results when applied to real-world scenes from SUN360. In contrast, our approach predicts sharper and more accurate details of local areas and finely-delineated object boundaries, significantly improving the holistic geometry understanding of the scene. We perform comprehensive experiments on public datasets to assess the effectiveness of our approach compared to state-of-the-art models. Our contributions are summarized as follows:

- We present *PanoNormal*, a specialized vision transformer architecture designed for estimating surface normals in monocular indoor ERP imagery. Notably, *PanoNormal* stands as the first panoramic transformer tailored for the 360° surface normal estimation task.
- *PanoNormal* seamlessly integrates the benefits of CNNs for robust low-level feature extraction, fortifying locality. Additionally, it harnesses the strengths of transformers in capturing long-range dependencies. The incorporation of a multi-scale scheme further enhances the holistic representation of the geometric structure within the scene.
- Extensive experiments have conducted on widely recognized benchmarks, namely 3D60, Stanford2D3D, Matterport3D, SunCG, and Structured3D. The results illustrate that *PanoNormal* consistently surpasses state-of-the-art approaches, and contributes to further studies in this domain by providing the first comprehensive evaluation across these public benchmarks.

2 Related Work

2.1 360° Surface Normal Estimation

Most existing methods [5, 7, 9] for surface normal estimation are designed for perspective images, which poses challenges, such as distortions, deformations, and domain shifts, that make conventional methods unsuitable for 360° images. Moreover, panoramic images introduce additional complexities to surface normal estimation, including variable illumination and intricate indoor layouts. Recent works can be broadly categorized into direct and indirect methods. Direct methods [11, 14, 16] introduce specific loss functions (e.g., spherical loss, hypersphere loss, double-quaternion loss) to comprehend the geometric structure on the unit sphere with various CNN architectures. [8] explicitly embed invariance against spherical distortions into CNNs, adjusting the sampling locations of convolutional filters to counter distortions and align the filters around the sphere effectively. Indirect methods [2, 27] draw inspiration from other vision tasks, e.g., 360° depth estimation, and adapt them for surface normal estimation. Work such as [13, 15, 18, 21] propose methodologies that project equirectangular images into corresponding CMP or tangent plane projection (TP) sub-images for predictions or directly learn internal correlations among these projections, aiming to capture details and holistic information concurrently with distortion awareness. However, employing simple CNNs with various spherical loss functions or adapting surface normal estimation methods from depth alone fails to yield satisfactory results. In addition, there are no surface normal estimation methods that provide a standardized evaluation across diverse public benchmarks, similar to the established practices in depth estimation tasks.

2.2 Vision Transformer

Vision transformers (ViTs) are a class of models that use self-attention mechanisms to process images as sequences of patches [10]. ViTs [12, 22, 27, 29] have
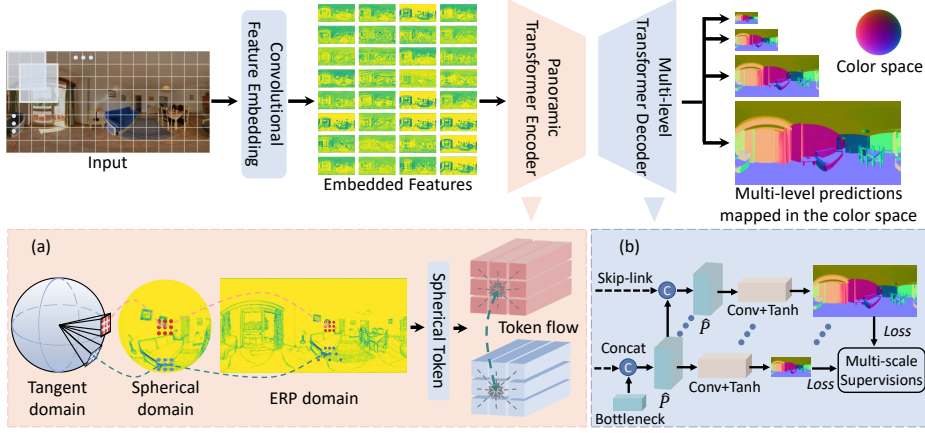
Fig. 2: Top: the overall architecture of the proposed *PanoNormal* method. Bottom: the key components: (a) The distortion-aware sampling process on the tangent patch, its transformation to the target ERP domain, and the application of a self-attention scheme among the tokens within each patch. A learnable token flow facilitates attention among the patches. (b) The proposed hierarchical multi-level transformer decoder, which produces results in different scales for comprehensive learning.

achieved remarkable results on conventional images captured by pinhole cameras, which have a limited field of view and which have, at most, mild distortions. In contrast, 360° images offer a complete, immersive view of the surrounding scene but require adaptations and modifications of the original ViTs to handle challenges such as significant image distortions, object deformation, and domain shifts. [18] and [15] proposed to divide patches on the spherical tangent domain into tangent tokens to reduce the negative effect of panoramic distortions, and introduced an attention module that considers both spatial and angular relations among tokens. [25] presented a panoramic ViT for saliency detection in 360° videos, which leverages a multi-scale feature fusion module and a temporal attention module to capture the spatial and temporal saliency cues. [26] proposed a method for panoramic semantic segmentation task, which is equipped with deformable patch embedding and deformable MLP modules for handling object deformations and image distortions, and also enhances the mutual prototypical adaptation strategy for unsupervised domain adaptive panoramic segmentation. These works demonstrate the potential and effectiveness of ViTs for 360° vision tasks and motivated us to investigate suitable ViTs for the surface normal dense prediction task, aiming to seamlessly integrate the strengths of the previously mentioned methods. Our objective is to yield robust evaluation results across benchmarks, contributing to further studies in this domain.

3   Our Method

To address the challenge of estimating surface normals using a single panoramic image for indoor scenes, we propose a novel architecture, *PanoNormal*. *PanoNor-*

mal leverages the capabilities of convolutional layers for extracting meaningful embeddings from panoramic images. To address the challenge of spherical distortion in 360° images while maintaining global dependencies, we crafted a U-shaped distortion-aware transformer architecture, drawing inspiration from the approach proposed by [18]. More specifically, we adopt a multi-level structure in our transformer decoder, capturing spatial relationships, processing fine-grained details, and integrating high-level contextual information across different levels. Fig. 2 illustrates the architecture of *PanoNormal*.

3.1 Network Architecture

Feature Embedding In a conventional ViT-based network, feature embedding undergoes processing through only a single convolutional layer before ViT blocks. It has been demonstrated that it works well for some 360° understanding tasks, such as depth estimation [18]. Nonetheless, although both depth estimation and surface normal tasks demand high-quality contextual information, surface normal tasks necessitate deeper features to effectively capture more useful cues, such as the orientation of objects. In contrast to the simplicity suitable for depth estimation, the intricate nature of surface normal requirements poses a challenge for the feature embedding achieved through a single convolutional layer, leading to sub-optimal results (quantitative results are shown in Tab. 1).
 To address this issue, we introduce a series of convolutional layers aimed at extracting more effective features. This approach enhances our model's ability to gain a more comprehensive understanding of the entire scene, improving performance in surface normal estimation. The feature embedding block consists of three 3×3 convolutional layers, each followed by a batch normalization function and a rectified linear unit (ReLU) activation function.

Distortion-aware Transformer Encoder The inherent non-uniform spatial warping of visual features, caused by spherical distortion in the 360° image, is alleviated by applying PanoFormer blocks, as introduced by [18]. To address issues such as distortions, misalignment, and inaccuracies arising from direct pixel sampling on the ERP image, a tangent projection (TP) division strategy is employed. It samples related surrounding pixels of the central pixel (tangent point) on each dense divided plane in the tangent domain, obtaining a series of tokens in patches with decent position representation that can be further transformed to the ERP domain. Subsequently, a conventional multi-head vision transformer block is applied, with the replacement of the feed-forward network (FFN) to the locally-enhanced feed-forward network (LeFF) [22, 24] for enhancing local feature interaction. The introduced encoder not only computes attention scores between central and correlated tokens but also integrates a trainable token flow. This token flow serves as a bias to adjust the spatial distribution of tokens, supplying the network with additional positional information for learning global dependencies. An example is shown in Fig. 2(a) and the representation of the

self-attention is as follows:

$$P(f, \hat{s}) = \sum_m W_m \left[\sum_{(q,k)} A_{mqk} \cdot W'_m f(\hat{s}_{mqk} + \Delta s_{mqk}) \right] \tag{1}$$

where the sampling strategy is adopted on the feature representations f, and is denoted as $\hat{s}$; m, q, k represent the self-attention head, each token, and its neighboring tokens in a tangent patch, respectively. W_m and W'_m denote the learnable weights of each head, A_{mqk} is the attention weights for each token, and Δs_{mqk} signifies the learned bias through of each token's query.

The learned embeddings P are subsequently transmitted through skip links to their respective hierarchical decoder blocks. Simultaneously, they undergo downsampling, reducing the feature size by half while doubling the dimensions, before proceeding to a bottleneck block for decoding.

Multi-level Transformer Decoder Our proposed ViT decoder, designed with spherical distortion awareness and a hierarchical structure to predict normal maps of different scales, is illustrated in Fig. 2(b). The proposed multi-level decoder comprises four independent blocks. Each block processes the concatenation of the upsampled encoded representations $\hat{f}_i$, featuring twice the spatial resolution size and halved the number of channels from the preceding level, and the directly propagated features $\hat{s}_i$ from the encoders through the skip-links. The surface normal vectors in various scales are generated as outputs using 3×3 convolutions, followed by a hyperbolic tangent (tanh) activation function to constrain them to the range $[-1, 1]$. This process can be described as:

$$\hat{\mathbf{N}}_i = \tanh \left(\hat{P}(\hat{f}_i, \hat{s}_i) \right) \tag{2}$$

where $\hat{\mathbf{N}}_i$ denotes the predicted surface normal maps for the i-th scale.

This architecture enhances feature analysis across fine and coarse scales, promoting a holistic comprehension of diverse granularities and elevating spatial understanding. It filters noise effectively, preserving essential features and enhancing generalization to unseen data. The significance of the introduced decoder in enhancing final predicted results has been validated through our ablation study (Sec. 4.4).

3.2   Loss Function

The presented network produces surface normal maps at various scales to capture a more comprehensive global geometry structure of the scene. In the training process, the predicted maps apply bilinear upsampling to align with the input size, followed by the adoption of the following losses:

MSE Loss: L_m, is the mean squared error between the ground truth and the predicted normals of each pixel, defined as:

$$L_m = \sum_{i=1}^{S} \|\hat{\mathbf{N}}_i - \mathbf{N}_i\|_2 \tag{3}$$

where S is the number of scales, and N_i denotes the ground truth surface normal maps for the i-th scale.

Quaternion Loss: L_q [14], measures the angular difference between predicted and ground truth normal maps on a pixel-wise basis:

$$L_q = \sum_{i=1}^{N} \sum_{j=1}^{M} \arctan(\frac{\|\hat{\mathbf{N}}_{ij} \times \mathbf{N}_{ij}\|}{\hat{\mathbf{N}}_{ij} \cdot \mathbf{N}_{ij}}) \tag{4}$$

where M indicates the number of pixels of the input, and j indexes the current pixel.

Perceptual Loss: L_p, is employed on the finest scales to enhance the generation of finer details:

$$L_p = l_{feat}^{\phi,k}(\hat{\mathbf{N}}, \mathbf{N}) = \sum_{j=1}^{M} \frac{1}{C_k M} \|\phi_k(\hat{\mathbf{N}}_j) - \phi_k(\mathbf{N}_j)\|_2^2 \tag{5}$$

where ϕ is the VGG-16 network [19] that pretrained on the ImageNet dataset [17], and C_k indicates C dimensional features for the k-th layer of the network ϕ.

Smooth Loss: L_s, quantifies the gradient G in the x and y directions in the ground truth and the predicted surface normal map at all scales:

$$L_s = \sum_{i=1}^{N} \sum_{j=1}^{M} (|G_{ij}^x| + |G_{ij}^y|) \tag{6}$$

The overall loss function of our network is:

$$L = \lambda_m L_m + \lambda_q L_q + \lambda_p L_p + \lambda_s L_s \tag{7}$$

By default, we set $\lambda_m = 1.0$, $\lambda_q = 10.0$, $\lambda_p = 0.05$, and $\lambda_s = 0.5$ as the weights for different terms. In our experiments, we observed that the use of these four loss functions and their respective weights consistently produced the best results in comparison to alternative loss combinations.

4   Experiments and Results

We adopted five popular panorama benchmark datasets for our experimental validation, both quantitatively and qualitatively. They are 3D60 [30], Stanford2D3D [3], Matterport3D [6], SunCG [20], and Structured3D [28]. In addition, SUN360 [23], which contains real-world data with no ground truth, was used for further qualitative and generalization comparison. We compared our method

with HyperSphere [14] which is the state-of-the-art for 360° surface normal estimation. In addition, we further adapt four popular 360° and perspective image depth estimation methods (PanoFormer [18], OmniFusion [15], MonoViT [27], UniFuse [13]) to the surface normal estimation task, to validate the effectiveness of our designed architecture. It is essential to note that the methods compared in this evaluation represent the current state-of-the-art in both 360° surface normal estimation and a highly relevant task, depth estimation. While HRDFuse [1] is acknowledged as the latest work in 360° depth estimation which employs a histogram bin approach to learn depth distribution, it is not suitable for adapting to surface normal tasks.

4.1   Evaluation Metric and Datasets

We conducted performance evaluation in surface normal estimation using three standard angular error metrics (mean error (Mean), median error (Median), and mean square error (MSE)), and five accuracy metrics that measure the percentage of pixels where the ratio (δ) between predicted surface normal vectors and ground truth is less than 5°, 7.5°, 11.5°, 22.5°, and 30°. A consistent setting is applied to ensure a fair comparison across all methods, and detailed specifics for each dataset are presented below.

3D60 The 3D60 dataset offers a broad spectrum of panoramic images with resolutions of 256×512 captured in varied environments. The captured 360° RGB imagery with corresponding information, such as surface normal and depth with specific camera positions are from two real-world indoor scanning environments, Stanford2D3D and Matterport3D, alongside synthetic scenes from the SunCG datasets. The inherent distribution gap among these datasets enhances the model's generalizability. To facilitate model training and evaluation, we adopt the data splits utilized in HyperSphere, as recommended in the official introduction. Notably, Matterport3D lacks ground truth data for 360° surface normals, and Stanford2D3D's surface normal instances lack consistently aligned axes across their data. Consequently, we evaluated them based on specific separations within the 3D60 dataset.

Structured3D Structured3D is a large-scale synthetic dataset featuring 21,835 512×1024 resolution of the panoramic data across 3500 scenes, encompassing RGB images illuminated with cold, normal, and warm lighting, as well as surface normal, depth, and semantic annotations. As [28] did not include any official training, validation and test splits, we preprocessed and formed the dataset examples with an 8:1:1 ratio, yielding 17,442 training data instances with three distinct lighting conditions (52,326 in total with three lighting conditions) and 2,179 and 2,181 validation and test data instances with randomly selected lighting conditions. For future convenience, the split files and the corresponding data loader are readily available in our project's Git repository.

4.2   Implementation Details

Our experiments were carried out utilizing a single CPU core of an Intel Xeon W-2133 paired with an RTX 3090 GPU, with a batch size configured to 2 and the input resolution set to 256×512. The chosen optimizer was Adam, with default settings maintained. The initial learning rate was 1×10^{-4}, decreasing by half every 15 epochs. We trained our model for 110 epochs and incorporated early stopping at the 15th epoch if there were no further improvements.

4.3   Experimental Results

We present a quantitative comparison among state-of-the-art methods, algorithms adapted for spherical surface normal estimation, and our *PanoNormal* model across five datasets, as detailed in Table 1. To ensure a fair evaluation, we retrained all models with identical settings. *PanoNormal* demonstrates superior performance, achieving a new state-of-the-art status across all five benchmarks. It showcases a consistent improvement of 9.31% for the mean error, 12.64% for the median error, and 14.01% for the mean square error (MSE) on average, outperforming the previous state-of-the-art methods highlighted in grey. In specific instances, our model demonstrates notable improvements in the MSE metric, achieving a 25.33% enhancement on 3D60, 19.73% on Stanford2D3D, 26.05% on Matterport3D, and 30.99% on SunCG. However, the improvement is only 2.69% on the Structured3D dataset with MSE. This difference is less significant compared to others due to the complex, synthetic nature of Structured3D scenes, which include numerous small objects with subtle curvature changes like ornaments, drawer handles, and wall-mounted kitchen tools. The dataset also presents challenges with intricate textures, as observed in items such as mirrors, glass walls, and carpets. In addition, *PanoNormal* exhibits a marginally higher median error compared to HyperSphere on the Stanford2D3D dataset, indicating potential sensitivity to outliers. However, this discrepancy also suggests that our method captures finer details, as HyperSphere sacrifices sharp boundaries in its predictions. The perceptibly more blurred outcomes from HyperSphere are illustrated in Fig. 3. The enhancement in δ performance underscores our model's capacity to achieve more accurate predictions, thereby highlighting its generalizability and effectiveness across diverse domains within the datasets, including both real-world and synthetic scenarios.

We also present qualitative results with the RGB input images and the corresponding predictions generated by various methods, followed by the ground truth surface normal map, illustrated in Fig. 3. We show one test example of each dataset with specific colors mapped to coordinate information, providing an intuitive representation of surface normals. Additionally, areas with unavailable data are denoted by grey on the surface normal map. The *PanoNormal* model stands out for its ability to capture finer details with sharper boundaries showcasing more sensitivity to the subtle surface curvatures.

To assess the generalizability of our method, we conduct surface normal estimation on real-world data and then compare our results with those obtained

Table 1: Quantitative comparisons on five benchmarks with PanoNormal, HyperSphere [14], PanoFormer [18], OmniFusion [15], MonoViT [27], and UniFuse [13]. We evaluate our method improvement against the existing methods that have consistently demonstrated strong performance, distinguished by their highlighting in grey. *We assess these datasets using the corresponding partitions of the 3D60 dataset.

Dataset	Method	Error metric ↓			Accuracy metric ↑				
		Mean	Median	MSE	$\delta < 5°$	$\delta < 7.5°$	$\delta < 11.5°$	$\delta < 22.5°$	$\delta < 30°$
3D60	UniFuse	6.7732	0.5438	279.9294	75.67	78.41	82.08	89.27	92.00
	PanoFormer	17.4997	6.5841	929.2326	50.34	54.75	60.28	72.39	77.68
	OmniFusion	7.9552	1.3555	313.8380	71.90	75.57	79.79	87.88	90.96
	MonoViT	6.6087	0.7666	250.8495	75.41	78.61	82.57	89.92	92.64
	HyperSphere	5.7836	**0.2660**	224.6234	76.95	79.61	83.49	90.83	93.47
	Ours	**4.9312**	0.2671	**167.7174**	**78.57**	**81.70**	**85.67**	**92.43**	**94.89**
	Ours-Improve	**14.74%**	−0.40%	**25.33%**	**1.62**	**2.09**	**2.18**	**1.61**	**1.43**
Stanford2D3D*	UniFuse	7.1787	0.5024	311.2060	75.82	78.27	81.74	88.18	90.96
	PanoFormer	17.5138	7.3950	875.6306	47.81	52.56	58.60	71.68	77.64
	OmniFusion	8.3031	1.3415	336.8175	71.89	75.61	79.81	87.04	90.11
	MonoViT	7.1019	0.7017	283.0693	75.27	78.10	81.80	88.59	91.46
	HyperSphere	6.2644	**0.2579**	257.0234	76.98	79.28	82.80	89.36	92.17
	Ours	**5.6199**	0.3213	**206.3081**	**77.66**	**80.26**	**83.84**	**90.61**	**93.44**
	Ours-Improve	**10.29%**	−24.59%	**19.73%**	**0.68**	**0.99**	**1.04**	**1.25**	**1.26**
Matterport3D*	UniFuse	7.4312	0.6747	299.1123	72.55	75.69	79.89	88.31	91.38
	PanoFormer	18.3752	7.4810	964.8379	47.26	51.87	57.75	70.82	76.47
	OmniFusion	8.6668	1.5917	337.1754	68.78	72.72	77.41	86.77	90.24
	MonoViT	7.2026	0.9168	266.8899	72.36	76.04	80.58	89.08	92.13
	HyperSphere	6.3794	0.3314	240.0956	73.79	76.90	81.39	90.04	93.01
	Ours	**5.4004**	**0.3182**	**177.5569**	**75.81**	**79.51**	**84.13**	**91.90**	**94.62**
	Ours-Improve	**15.35%**	**3.99%**	**26.05%**	**2.02**	**2.61**	**2.74**	**1.86**	**1.61**
SunCG*	UniFuse	3.6620	0.0430	170.4886	88.43	89.76	91.47	94.33	95.55
	PanoFormer	14.0398	2.3807	838.0308	64.73	67.96	71.66	79.19	82.50
	OmniFusion	4.6781	0.3927	195.2205	84.84	87.32	89.66	93.27	94.79
	MonoViT	3.6754	0.2126	153.2902	88.11	89.70	91.55	94.65	95.88
	HyperSphere	2.8576	0.0035	129.4394	89.99	91.16	92.81	95.51	96.59
	Ours	**2.3221**	**0.0027**	**89.3309**	**90.86**	**92.13**	**93.78**	**96.41**	**97.43**
	Ours-Improve	**18.74%**	**23.62%**	**30.99%**	**0.86**	**0.97**	**0.97**	**0.90**	**0.84**
Structured3D	UniFuse	8.2525	0.3342	453.1296	76.24	81.43	83.52	87.55	89.54
	PanoFormer	16.9159	4.4362	1053.5312	59.13	64.10	68.29	75.50	78.86
	OmniFusion	20.7000	14.3028	831.9758	28.51	35.35	45.06	63.55	72.52
	MonoViT	5.9222	**0.1005**	277.8236	78.93	84.20	86.40	90.58	92.57
	HyperSphere	5.7865	0.1410	253.3796	78.38	83.68	86.12	90.73	92.88
	Ours	**5.5622**	0.1048	**246.5729**	**79.18**	**84.48**	**86.68**	**91.01**	**93.08**
	Ours-Improve	**3.88%**	25.67%	**2.69%**	**0.79**	**0.80**	**0.55**	**0.28**	**0.19**
Ours Average Improvement		**9.31%**	**12.64%**	**14.01%**	**1.21**	**1.45**	**1.37**	**0.95**	**0.81**

using Hypersphere. As demonstrated in Fig. 4, *PanoNormal* produces precise predictions on the unseen real-world SUN360 dataset. It accurately estimates the complete boundaries of various objects, even in the presence of distortions and complex textures. Noteworthy examples include the bed at the bottom of the ERP image in the first column and the glass door in the third column. In contrast, the model of HyperSphere does not generalize well to real-world panoramic images. These observations provide further validation of the efficacy of our proposed methods. Furthermore, when examining Stanford2D3D and Matterport3D
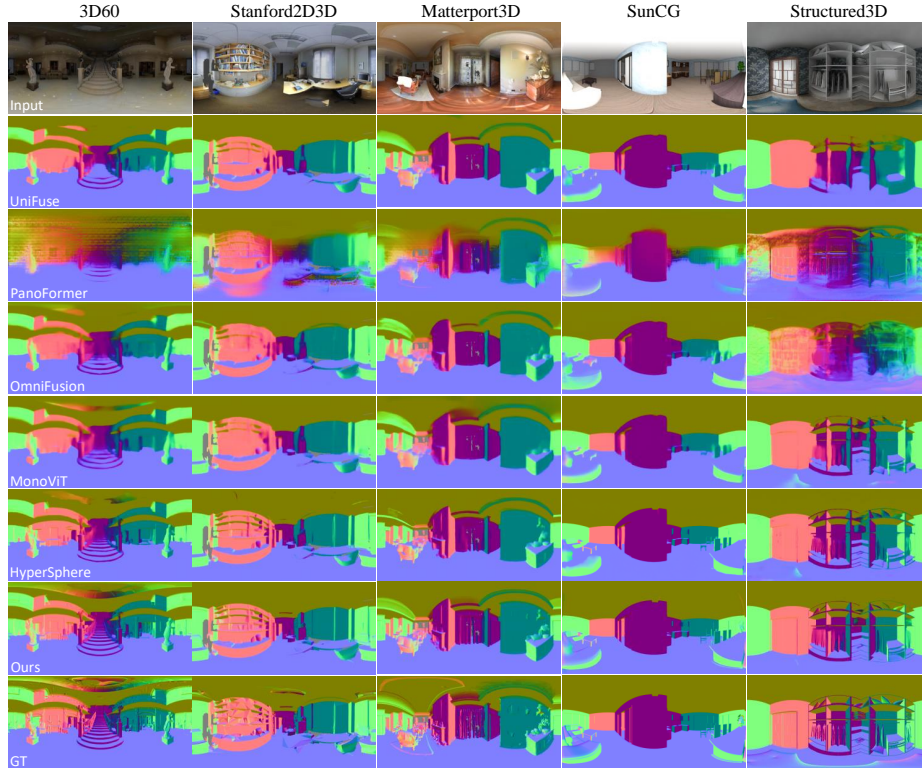
Fig. 3: Qualitative comparisons across five benchmarks, featuring *PanoNormal*, UniFuse, PanoFormer, OmniFusion, MonoViT, and HyperSphere. Optimal viewing experience in color.

Table 2: Ablation study.

Method	**P**ano**F**ormer	PF-R1	Ours	Ours-R1	Ours-R2	Ours-R3	Ours-R4
Mean ↓	17.500	5.154	4.931	5.310	5.337	5.305	5.506
Median ↓	6.584	0.321	0.267	0.394	0.383	0.358	0.398
MSE ↓	929.233	178.146	167.717	183.356	186.472	184.613	193.994

as real-world datasets, it is important to acknowledge that their ground truth surface normal map is constructed with triangle faces, and may present certain visual characteristics. However, our method demonstrates a capability for generating smooth surface normals, providing enhanced precision in defining boundaries. This improvement contributes to an elevated standard of visual quality in our results.

4.4   Ablation Study

In our comprehensive evaluation under identical conditions, we conducted an ablation study on the 3D60 dataset to validate the key components of our model.
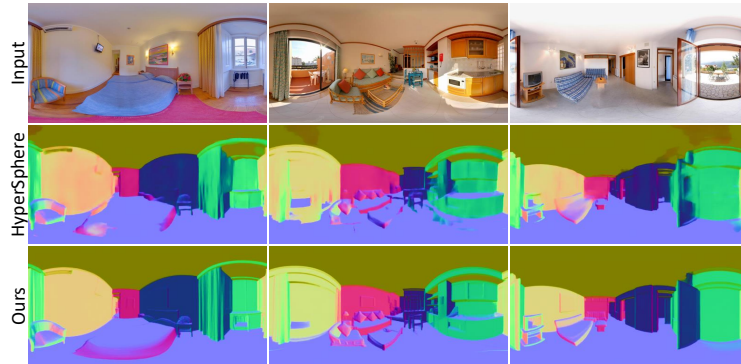
Fig. 4: Normal estimation predictions on some real-world data. The images are from the SUN360 [23] dataset. More qualitative results can be found in our supplementary materials.

As presented in Table 2, PanoFormer serves as the baseline structure for surface normal prediction, adapted from depth estimation methods. Introducing the multi-level decoder in the first placement of PanoFormer results in a notable decrease in mean, median, and MSE error metrics by **70.55%**, **95.12%**, and **80.83%**, respectively. Our network, featuring another proposed feature embedding component, emerges as the top-performing configuration among ablation experiments, achieving state-of-the-art performance by another improvement with 4.32% on the mean, **16.84% on the median**, and 5.85% on MSE. The "Replace 1 − 4" scenario, where convolutional layers replace self-attention blocks symmetrically in both the encoder and decoder, demonstrates promising results. Specifically, the third placement, maintaining the self-attention block only at the bottleneck and one level higher in both the encoder and decoder, achieves the second-best performance on average. This configuration holds potential for real-world applications with limited device resources, offering advantages in terms of reduced memory space, faster training, and quicker inferencing times. Fig. 5 illustrates qualitative comparisons among our ablation architectures. In the first row, we display the input panoramic images along with their corresponding ground truth surface normals. The following rows depict the normalized absolute error between the predicted surface normal map and the ground truth map. In these rows, darker shades of red indicate higher error, alongside the corresponding predicted surface normal maps. Once more, it is evident that our current architecture exhibits superior performance when confronted with diverse challenging scenarios.

Furthermore, our proposed architecture consistently outperforms PanoFormer [18] across all metrics, both quantitatively and qualitatively, on every dataset. The adapted PanoFormer implementation yields less satisfactory results in all comparisons, encountering notable challenges on the Structured3D synthetic dataset and struggling with convergence. In contrast, our *PanoNormal* framework consistently demonstrates outstanding performance across all datasets, highlighting the efficacy and significance of the proposed architecture.
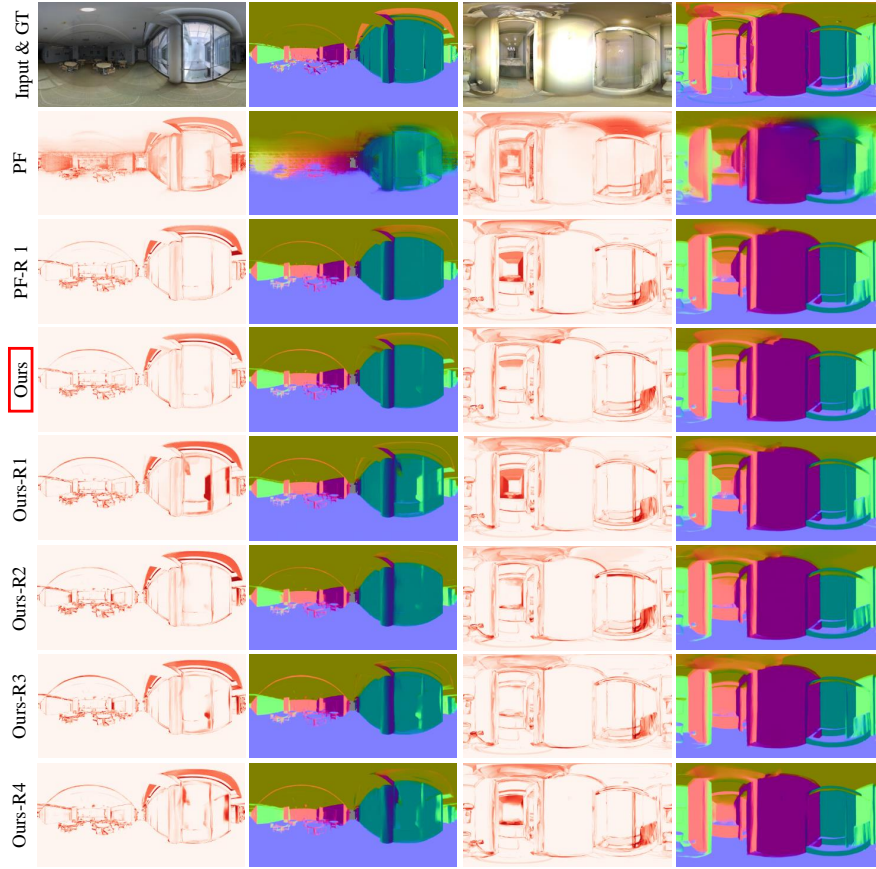
Fig. 5: Qualitative comparisons among our ablation architectures. Top row: RGB inputs and the ground truth surface normal maps. Subsequent rows: the experiment architectures with predicted surface normals and corresponding error maps, where darker shades of red signify more pronounced errors. Optimal viewing experience in color.
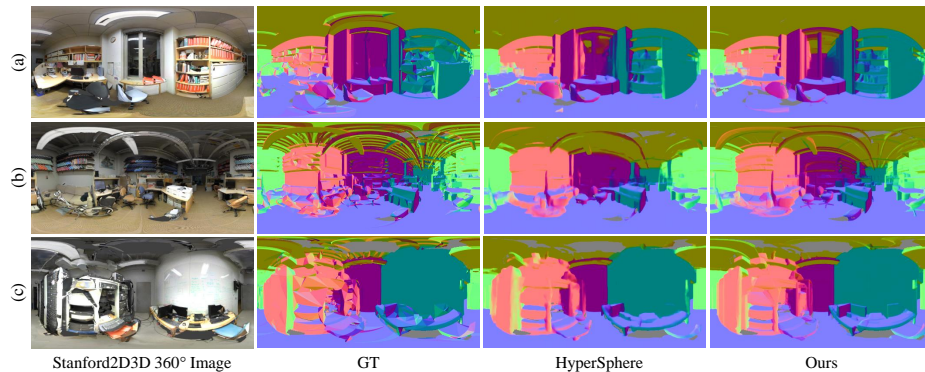
4.5   Limitation

In Table 1, our method exhibits a performance of approximately 24.59% higher median error compared to HyperSphere on the Stanford2D3D dataset while demonstrating significant improvements in the metrics of mean and MSE. The enhancements on mean and MSE suggest that, on average, our model provides more accurate predictions. However, the higher median error implies the existence of a subset of predictions with larger errors.

To investigate the factors contributing to the higher median error, we inspected the predicted results. We present three typical cases from the Stanford2D3D dataset, both quantitatively in Tab. 3 and qualitatively in Fig. 6. Notably, the ground truth surface normal data in the Stanford2D3D dataset is generated based on the reconstructed triangular mesh of each real-world scene.

Table 3: Specific examples from Stanford2D3D dataset.

Example	Method	Mean ↓	Median ↓	MSE ↓	$\delta < 7.5°$	$\delta < 22.5°$	$\delta < 30°$
(a)	HyperSphere	10.5388	0.0656	470.1378	66.24	82.44	86.18
	Ours	10.4650	0.0816	450.3420	66.57	82.43	86.70
(b)	HyperSphere	16.8774	7.6914	753.1895	49.69	68.10	75.56
	Ours	16.1840	8.8487	634.5417	47.76	68.10	76.95
(c)	HyperSphere	13.2489	0.8248	564.9490	57.08	77.85	83.39
	Ours	12.2771	2.3333	473.4669	58.34	79.36	84.92

Stanford2D3D 360° Image   GT   HyperSphere   Ours

Fig. 6: Qualitative evaluation on three specific examples.

Predictions aligning with surfaces constructed with triangles may deviate from the authentic appearance of objects. HyperSphere, in such instances, blurs object boundaries and achieves a lower median error on such regions, while our approach predicts a more precise boundary that better aligns with the actual shape of objects. This distinction contributes to the overall higher median error, attributed to the inherent limitations in the quality of the ground truth data.

5   Conclusion

We present, *PanoNormal*, a deep architecture designed for single 360° surface normal estimation. Our approach leverages the combined strengths of convolutional neural Networks for the effective capture of local details and spherical vision transformers for global dependency with distortion awareness. Our experiments demonstrate the effectiveness of our framework. *PanoNormal* exhibits significant advances over state-of-the-art methods across five popular 360° panoramic datasets. Additionally, *PanoNormal* demonstrates enhanced generalizability compared to previous works, and our ablation studies reinforce the efficacy of our proposed architecture and indicate its potential applicability in real-world scenarios. In the future, we will investigate the utility of our deep

architecture that combines spherical transformers and convolutional operations in other 360° regression tasks.

References

1. Ai, H., Cao, Z., Cao, Y.P., Shan, Y., Wang, L.: HRDFuse: Monocular 360deg depth estimation by collaboratively learning holistic-with-regional depth distributions. In: Proceedings of the IEEE/CVF Conference on Computer Vision and Pattern Recognition. pp. 13273–13282 (2023) 8
2. Albanis, G., Zioulis, N., Drakoulis, P., Gkitsas, V., Sterzentsenko, V., Alvarez, F., Zarpalas, D., Daras, P.: Pano3D: A holistic benchmark and a solid baseline for 360° depth estimation. In: Proceedings of the IEEE/CVF Conference on Computer Vision and Pattern Recognition. pp. 3727–3737 (2021) 3
3. Armeni, I., Sax, S., Zamir, A.R., Savarese, S.: Joint 2d-3d-semantic data for indoor scene understanding. arXiv preprint arXiv:1702.01105 (2017) 7
4. Bae, G., Budvytis, I., Cipolla, R.: Estimating and exploiting the aleatoric uncertainty in surface normal estimation. In: International Conference on Computer Vision (ICCV) (2021) 1
5. Bae, G., Budvytis, I., Cipolla, R.: Estimating and exploiting the aleatoric uncertainty in surface normal estimation. In: Proceedings of the IEEE/CVF International Conference on Computer Vision. pp. 13137–13146 (2021) 3
6. Chang, A., Dai, A., Funkhouser, T., Halber, M., Niessner, M., Savva, M., Song, S., Zeng, A., Zhang, Y.: Matterport3D: Learning from rgb-d data in indoor environments. arXiv preprint arXiv:1709.06158 (2017) 7
7. Chen, Z., Shen, Y., Ding, M., Chen, Z., Zhao, H., Learned-Miller, E.G., Gan, C.: Mod-Squad: Designing mixtures of experts as modular multi-task learners. In: Proceedings of the IEEE/CVF Conference on Computer Vision and Pattern Recognition (CVPR). pp. 11828–11837 (June 2023) 3
8. Coors, B., Condurache, A.P., Geiger, A.: SphereNet: Learning spherical representations for detection and classification in omnidirectional images. In: Proceedings of the European conference on computer vision (ECCV). pp. 518–533 (2018) 2, 3
9. Do, T., Vuong, K., Roumeliotis, S.I., Park, H.S.: Surface normal estimation of tilted images via spatial rectifier. In: Computer Vision–ECCV 2020: 16th European Conference, Glasgow, UK, August 23–28, 2020, Proceedings, Part IV 16. pp. 265–280. Springer (2020) 3
10. Dosovitskiy, A., Beyer, L., Kolesnikov, A., Weissenborn, D., Zhai, X., Unterthiner, T., Dehghani, M., Minderer, M., Heigold, G., Gelly, S., et al.: An image is worth 16x16 words: Transformers for image recognition at scale. arXiv preprint arXiv:2010.11929 (2020) 3
11. Feng, B.Y., Yao, W., Liu, Z., Varshney, A.: Deep depth estimation on 360 images with a double quaternion loss. In: 2020 International Conference on 3D Vision (3DV). pp. 524–533. IEEE (2020) 3
12. Jain, J., Singh, A., Orlov, N., Huang, Z., Li, J., Walton, S., Shi, H.: SeMask: Semantically masked transformers for semantic segmentation. In: Proceedings of the IEEE/CVF International Conference on Computer Vision. pp. 752–761 (2023) 3
13. Jiang, H., Sheng, Z., Zhu, S., Dong, Z., Huang, R.: UniFuse: Unidirectional fusion for 360 panorama depth estimation. IEEE Robotics and Automation Letters **6**(2), 1519–1526 (2021) 1, 3, 8, 10

14. Karakottas, A., Zioulis, N., Samaras, S., Ataloglou, D., Gkitsas, V., Zarpalas, D., Daras, P.: 360 surface regression with a hyper-sphere loss. In: 2019 International Conference on 3D Vision (3DV). pp. 258–268. IEEE (2019) 2, 3, 7, 8, 10

15. Li, Y., Guo, Y., Yan, Z., Huang, X., Duan, Y., Ren, L.: OmniFusion: 360 monocular depth estimation via geometry-aware fusion. In: Proceedings of the IEEE/CVF Conference on Computer Vision and Pattern Recognition. pp. 2801–2810 (2022) 2, 3, 4, 8, 10

16. Liao, S., Gavves, E., Snoek, C.G.: Spherical Regression: Learning viewpoints, surface normals and 3d rotations on n-spheres. In: Proceedings of the IEEE/CVF Conference on Computer Vision and Pattern Recognition. pp. 9759–9767 (2019) 1, 2, 3

17. Russakovsky, O., Deng, J., Su, H., Krause, J., Satheesh, S., Ma, S., Huang, Z., Karpathy, A., Khosla, A., Bernstein, M., et al.: Imagenet large scale visual recognition challenge. International journal of computer vision **115**, 211–252 (2015) 7

18. Shen, Z., Lin, C., Liao, K., Nie, L., Zheng, Z., Zhao, Y.: PanoFormer: Panorama transformer for indoor 360° epth estimation. In: European Conference on Computer Vision. pp. 195–211. Springer (2022) 2, 3, 4, 5, 8, 10, 12

19. Simonyan, K., Zisserman, A.: Very deep convolutional networks for large-scale image recognition. arXiv preprint arXiv:1409.1556 (2014) 7

20. Song, S., Yu, F., Zeng, A., Chang, A.X., Savva, M., Funkhouser, T.: Semantic scene completion from a single depth image. In: Proceedings of the IEEE conference on computer vision and pattern recognition. pp. 1746–1754 (2017) 7

21. Wang, F.E., Yeh, Y.H., Tsai, Y.H., Chiu, W.C., Sun, M.: BiFuse++: Self-supervised and efficient bi-projection fusion for 360 depth estimation. IEEE Transactions on Pattern Analysis and Machine Intelligence **45**(5), 5448–5460 (2022) 3

22. Wang, Z., Cun, X., Bao, J., Zhou, W., Liu, J., Li, H.: UFormer: A general u-shaped transformer for image restoration. In: Proceedings of the IEEE/CVF conference on computer vision and pattern recognition. pp. 17683–17693 (2022) 3, 5

23. Xiao, J., Ehinger, K.A., Oliva, A., Torralba, A.: Recognizing scene viewpoint using panoramic place representation. In: 2012 IEEE Conference on Computer Vision and Pattern Recognition. pp. 2695–2702. IEEE (2012) 2, 7, 12

24. Yuan, K., Guo, S., Liu, Z., Zhou, A., Yu, F., Wu, W.: Incorporating convolution designs into visual transformers. In: Proceedings of the IEEE/CVF International Conference on Computer Vision. pp. 579–588 (2021) 5

25. Yun, H., Lee, S., Kim, G.: Panoramic vision transformer for saliency detection in 360° ideos. In: European Conference on Computer Vision. pp. 422–439. Springer (2022) 4

26. Zhang, J., Yang, K., Ma, C., Reiß, S., Peng, K., Stiefelhagen, R.: Bending Reality: Distortion-aware transformers for adapting to panoramic semantic segmentation. In: Proceedings of the IEEE/CVF Conference on Computer Vision and Pattern Recognition (CVPR). pp. 16917–16927 (June 2022) 4

27. Zhao, C., Zhang, Y., Poggi, M., Tosi, F., Guo, X., Zhu, Z., Huang, G., Tang, Y., Mattoccia, S.: MonoVit: Self-supervised monocular depth estimation with a vision transformer. In: 2022 International Conference on 3D Vision (3DV). pp. 668–678. IEEE (2022) 3, 8, 10

28. Zheng, J., Zhang, J., Li, J., Tang, R., Gao, S., Zhou, Z.: Structured3D: A large photo-realistic dataset for structured 3d modeling. In: Computer Vision–ECCV 2020: 16th European Conference, Glasgow, UK, August 23–28, 2020, Proceedings, Part IX 16. pp. 519–535. Springer (2020) 7, 8

29. Zhu, L., Wang, X., Ke, Z., Zhang, W., Lau, R.W.: BiFormer: Vision transformer with bi-level routing attention. In: Proceedings of the IEEE/CVF Conference on Computer Vision and Pattern Recognition (CVPR). pp. 10323–10333 (June 2023) 3
30. Zioulis, N., Karakottas, A., Zarpalas, D., Daras, P.: OmniDepth: Dense depth estimation for indoors spherical panoramas. In: Proceedings of the European Conference on Computer Vision (ECCV). pp. 448–465 (2018) 7